Dynamics of dendritic sidebranching in the two-dimensional symmetric model of solidification

Michael N. Barber,* Angelo Barbieri, and J. S. Langer
Institute for Theoretical Physics, University of California, Santa Barbara, California 93106
(Received 23 March 1987)

We study, within a WKB approximation, the evolution of time-dependent deformations of the needle crystal solution of the two-dimensional symmetric model of solidification. We find that perturbations with fixed small frequencies are initially amplified as they propagate from near the tip down the dendrite but ultimately decay. Localized wave packets behave rather differently; the packet continues to grow exponentially as it moves to arbitrarily large distances from the tip. The relevance of these results to sidebranching of dendrites is discussed.

I. INTRODUCTION

Considerable progress has been made in the last few years in understanding the mechanisms of mode selection in dendritic growth of a pure solid from its undercooled melt. (For a recent review, see Langer.[1]) Recent work has established that surface tension acts as a singular perturbation in this problem. In the absence of surface tension, an infinite continuous family of needle crystal solutions—the Ivantsov[2] solutions—exist for any given undercooling. Inclusion of surface tension leads to the selection, via a solvability condition, of a particular steady-state solution that deviates slightly from an Ivantsov solution. This mechanism was first discovered in simpler local models.[3,4,5,6] Subsequently, it has been confirmed both numerically[7,8] and analytically[9,10,11,12] in more realistic nonlocal models, in particular the so-called symmetric model,[1,13] which contains a completely realistic description of the thermal field.

In this paper we extend the analytical techniques of Barbieri *et al.*[10] for the steady-state selection problem to the dynamic problem of sidebranching of the steady-state needle crystal solution of the two-dimensional symmetric model. A numerical study of this problem has been reported recently by Kessler and Levine.[14] We are able to reproduce quantitatively many of the features found in the numerical solution by a WKB solution. The numerical solution refers to the propagation of a perturbation of fixed frequency. Using the WKB solutions we are able to go further and consider the evolution of a localized (in space) wave packet as it moves along the dendrite. We find that the behavior of such a packet is qualitatively different from that of a single mode. In particular, we recover the same behavior as found by Pieters and Langer[15] in the local boundary-layer model.[4]

The paper is arranged as follows. In Sec. II, we first briefly review the formulation of the symmetric model to establish notation and then derive a linearized equation of motion for (small) time-dependent perturbations of the steady-state solution. Section III contains the solution of this equation by a WKB technique. This solution is compared quantitatively with the numerical solution of Kessler and Levine in Sec. IV. In Sec. V, we discuss the motion of a wave packet and compare with the results of the boundary layer model. The paper closes with an overall summary in Sec. VI, where we also comment on the relation of our calculation with recent similar work, in particular that of Bensimon *et al.*[16] and Caroli *et al.*[17]

II. TIME-DEPENDENT PERTURBATIONS IN THE SYMMETRIC MODEL

We consider the symmetric model in two dimensions and let $\zeta=\zeta(x,t)$ be the instantaneous position of the solidification front, which we assume to be moving in the positive z direction with velocity v. As usual it is convenient to measure lengths in units of ρ, the radius of curvature of the tip, and times in units of ρ/v. The evolution equation for the front is standard[1,13] and in our scaled units can be written

$$\Delta-\frac{d_0}{\rho}\kappa[\zeta(x,t)]=p\int_0^\infty\frac{d\tau}{2\pi\tau}\int_{-\infty}^{\infty}dx'[1+\dot\zeta(x',t-\tau)]\exp\left[-\frac{p}{2\tau}\{(x-x')^2+[\zeta(x,t)-\zeta(x',t-\tau)+\tau]^2\}\right], \tag{2.1}$$

where $\dot\zeta=\partial\zeta/\partial t$ and

$$\kappa[\zeta]=-\frac{\partial^2\zeta/\partial x^2}{[1+(\partial\zeta/\partial x)^2]^{3/2}} \tag{2.2}$$

is the curvature. The other quantities in (2.1) have their usual meanings. Specifically, $p=v\rho/2D$ is the thermal Péclet number with D the diffusion constant, which is equal in both phases, $\Delta=(T_M-T_\infty)/(L/c)$ is the di-

mensionless undercooling, where T_M is the melting temperature, T_∞ is the temperature infinitely far from the front, L is the latent heat, and c is the specific heat. The Gibbs-Thomson correction,[13] $d_0\kappa/\rho$, is determined by the capillary length $d_0=\gamma T_M c/L^2$, where γ is the surface tension. It is this term that is the singular perturbation. Physically, the left-hand side of (2.1) is thus the local equilibrium expression for the dimensionless temperature along the solidification front. The right-hand side of (2.1) is this same temperature obtained by directly solving the diffusion problem with the front acting as a line source of differential strength $(1+\dot{\zeta})dx$, the kernel being the Green's function for two-dimensional diffusion.

At zero surface tension, the steady-state solution of (2.1) is the Ivantsov parabola[1,13,11]

$$\zeta_{iv}(x)=-\tfrac{1}{2}x^2 , \tag{2.3}$$

where p and Δ are related by

$$\Delta(p)=2\sqrt{p}\,e^p\int_{\sqrt{p}}^{\infty} e^{-y^2}dy \simeq \sqrt{\pi p}\ , \quad p\to 0 . \tag{2.4}$$

In the presence of nonzero surface tension this solution is modified by a shape correction $\zeta_0(x)$ which is formally small in terms of the dimensionless parameter

$$\sigma=d_0/p\rho . \tag{2.5}$$

However, as discussed in detail in Refs. 10 and 11, this correction only exists if σ takes a special value σ^* determined by a microscopic solvability condition. Anisotropy plays a crucial role in this steady-state selection. We shall, however, assume that anisotropy is no longer essential for a discussion of time-dependent perturbations, such as sidebranching, of the steady-state solution *once this has been selected.*

Experimentally, σ is of order 0.02 so that the exact steady-state solution is very close to the Ivantsov solution. Thus we linearize (2.1) about ζ_{iv} by writing

$$\zeta(x,t)=-\tfrac{1}{2}x^2+\zeta_0(x)+\zeta_1(x,t) , \tag{2.6}$$

where both ζ_0 and ζ_1 are small for small σ. We assume that with the correct choice of σ as discussed above, the smooth shape correction ζ_0 cancels out of the linearization of (2.1). The result is a homogeneous equation for $\zeta_1(x,t)$ linear in $\partial/\partial t$. It is natural then to Fourier transform, where we define

$$\hat{\zeta}_1(x,\omega)=\int_{-\infty}^{\infty} e^{-i\omega t/\sqrt{\sigma}}\zeta_1(x,t)dt . \tag{2.7}$$

Physically, this definition of the frequency as $\omega/\sqrt{\sigma}$ implies that the characteristic timescale for motion of ζ_1 is of order $\sqrt{\sigma}$. We shall see later that mathematically this is the appropriate timescale. However, it is useful, at this point, to briefly consider the *physically* relevant timescales. From the diffusion Green's function in (2.1), we observe that the characteristic time of the thermal field is p or, in dimensional units, $p\rho/v=\rho^2/2D$, which is just the diffusion time for length scales of order ρ, the tip radius. The other time scale that presumably enters the problem is that associated with motion of the stability front itself. The linear stability analysis of Mullins and Sekerka[18,1,13] suggests that this time is λ_s/v, where λ_s is a stability length of order $\sqrt{d_0 D/v}$. In our dimensionless units this time is thus of order $\sqrt{\sigma}$. Hence, we can make a quasistationary approximation and neglect the τ dependence of ζ_1 and $\dot{\zeta}_1$ in (2.1) if $p\ll\sqrt{\sigma}$; a condition that is generally satisfied experimentally.

With this approximation, we find $\hat{\zeta}_1(x,\omega)$ satisfies

$$-\sigma\kappa_1\hat{\zeta}_1=\int_0^\infty\frac{d\tau}{2\pi\tau}\int_{-\infty}^{\infty}dx'\left[i\frac{\omega}{\sqrt{\sigma}}\hat{\zeta}_1(x',\omega)+\frac{p}{2\tau}[x^2-(x')^2-2\tau][\hat{\zeta}_1(x,\omega)-\hat{\zeta}_1(x',\omega)]\right]$$
$$\times\exp\left\{-\frac{p}{2\tau}\left[(x-x')^2+\left[\frac{(x')^2}{2}-\frac{x^2}{2}+\tau\right]^2\right]\right\} , \tag{2.8}$$

where κ_1 is the linearized curvature operator defined by

$$\kappa_1=-\frac{1}{(1+x^2)^{3/2}}\frac{d^2}{dx^2}+\frac{3x}{(1+x^2)^{5/2}}\frac{d}{dx} . \tag{2.9}$$

The integral on the right-hand side of (2.8) involving $\hat{\zeta}_1(x,\omega)$ can be computed explicitly.[12] The remaining integral over τ can be evaluated in terms of the Bessel functions of the third kind, $K_0(z)$ and $K_1(z)$, providing the resulting singular integral is interpreted as a Cauchy principal value, which we denote by $\mathrm{P}\int$. The resulting equation of motion reads:

$$-\sigma\kappa_1\hat{\zeta}_1+\frac{\hat{\zeta}_1}{1+x^2}=\left[\frac{i\omega}{\sqrt{\sigma}}+p\right]Z_0+Z_1 , \tag{2.10}$$

with

$$Z_0=\frac{1}{\pi}\int_{-\infty}^{\infty}dx'\,e^{-p[x'^2-x^2]/2}\hat{\zeta}_1(x',\omega)K_0(p\sqrt{\eta(x,x')}) , \tag{2.11}$$

and

$$Z_1=\frac{p}{2\pi}\mathrm{P}\int_{-\infty}^{\infty}dx'[(x')^2-x^2]e^{-p[(x'^2-x^2]/2}\hat{\zeta}_1(x',\omega)[\eta(x,x')]^{-1/2}K_1(p\sqrt{\eta(x,x')}) , \tag{2.12}$$

where

$$\eta(x,x')=(x-x')^2[1+\tfrac{1}{4}(x+x')^2] . \tag{2.13}$$

Equation (2.10) forms the basis of our subsequent analysis. It is worth emphasizing that the only approximations made in deriving it from (2.1) are the linearization about the Ivantsov parabola and the quasistationary approximation.

III. WKB SOLUTION

To proceed further and obtain an *analytical* solution of (2.10), we will take advantage of the fact that the experimentally relevant values of σ and p are much less than unity; typically $\sigma\sim 0.02$, and $p\leq 5\times 10^{-2}$. In addition, as discussed above, the quasistationary approximation requires $p\ll\sqrt{\sigma}$. Thus it is reasonable theoretically to consider the limit $p\to 0$. However, this limit is delicate because of the logarithmic divergence at small argument of K_0. Unlike in the steady-state calculation[10] (or in the derivation[19] of the corresponding dynamical equation in three dimensions), we cannot simply set $p=0$. We can, however, evaluate the integrals in (2.11) and (2.12) by an extension of the method used in the steady-state calculation, which avoids the apparent problems for $p=0$.

The essential idea is the same. We endeavour to replace the integral operators by local terms by assuming that $\hat{\xi}_1(x,\omega)$ has a WKB form governed by the singular parameter σ:

$$\hat{\xi}(x,\omega)\simeq\exp[iW(x,\omega)/\sqrt{\sigma}] \tag{3.1}$$

with

$$W(x,\omega)=W_0(x,\omega)+\sqrt{\sigma}W_1(x,\omega)+\cdots \tag{3.2}$$

and solve explicitly for W_0 and W_1.

With this substitution for $\hat{\xi}_1$, we perform the integrations over x' by deforming the contour of integration, which originally runs along the real axis, into the complex x' plane. As in the steady-state calculation, we do not know *a priori* whether to bend into the upper or lower half plane but need to check for self-consistency of the resulting solutions. The required consistency condition is that the modulus of the WKB solution decreases exponentially in the direction in which the contour is bent. In bending the contour we must take note of the singularity of the integrands at $x'=x$. In (2.12) this is a simple pole, but in Z_0, (2.11), we have a logarithmic branch point arising from $K_0(p\sqrt{\eta})\simeq-\ln|x-x'|$ as $x'\to x$. The associated branch cuts are most conveniently defined by the regularization $\ln|x-x'|\to\ln[(x-x')^2+\epsilon^2]^{1/2}$, $\epsilon\to 0^+$, resulting in a double cut structure.

For small σ we expect these singularities to yield the dominant contributions to the integrals; the remainder of the contour contributing exponentially small (in $\sqrt{\sigma}$) corrections. In the steady-state discussion[10] of the solvability condition, the justification of this estimate relied on the existence of saddle points in the analogue of $W(x,\omega)$ at $x=\pm i$ with $\mathrm{Im}W>0$. Here we will find that $\mathrm{Im}W(x,\omega)=0$ for pure imaginary x. Nevertheless, it will transpire that we can deform the contour in both (2.11) and (2.12) to a new contour along which $\mathrm{Im}W(x',\omega)$ is a minimum for $x'=x$.

It is possible to carry out this procedure directly on (2.11) by explicitly integrating along the relevant branch cut arising from $K_0(p\sqrt{\eta})$. It is, however, more convenient to deal with the logarithmic branch cut in Z_0 by differenting (2.10) with respect to x to obtain

$$-\sigma\frac{d}{dx}(\kappa_1\hat{\xi}_1)+\frac{d}{dx}\left[\frac{\hat{\xi}_1}{1+x^2}\right]=\left[\frac{i\omega}{\sqrt{\sigma}}+p\right](pxZ_0-\tilde{Z}_0)+\frac{dZ_1}{dx} , \tag{3.3}$$

where

$$\tilde{Z}_0=\frac{p}{2\pi}\mathrm{P}\int_{-\infty}^{\infty}dx'[\partial\eta(x,x')/\partial x]e^{-p[(x'^2-x^2)]/2}\hat{\xi}_1(x',\omega)[\eta(x,x')]^{-1/2}K_1(p\sqrt{\eta(x,x')}) , \tag{3.4}$$

We may now take the limit $p\to 0$. Hence, on using the fact that $K_1(z)\sim z^{-1}$ as $z\to 0^+$, Z_1 and $\tilde{Z}_0$ both become of the form

$$F[\hat{\xi}_1]=\mathrm{P}\int_{-\infty}^{\infty}dx'\frac{f(x',x)\hat{\xi}_1(x',\omega)}{x-x'} , \tag{3.5}$$

where $f(x',x)$ is regular at $x'=x$.

Inserting (3.1) for $\hat{\xi}_1$, we can evaluate F by deforming the contour as described above. From the pole at $x'=x$ we obtain

$$F[\hat{\xi}_1^{\pm}]\approx\mp\pi i f(x,x)\hat{\xi}_1^{\pm}(x,\omega) , \tag{3.6}$$

where the $+$ $(-)$ sign refers to the contribution arising from deforming the contour into the upper (lower) half plane. To ensure that the remainder of the contour does not contribute, we require that

$$\pm\mathrm{Re}W^{\pm\prime}(x)>0 . \tag{3.7}$$

Here and below the prime denotes differentiation with respect to x.

Applying the result (3.6) to Z_1 and $\tilde{Z}_0$ in the limit $p\to 0$, reduces (3.3) to a *local* ordinary differential equation for $\hat{\xi}_1^{\pm}$, namely

$$-\sigma^{3/2}\frac{d}{dx}(\kappa_1\hat{\xi}_1^{\pm})+\sigma^{1/2}\frac{d}{dx}\left[\frac{1\mp ix}{1+x^2}\hat{\xi}_1^{\pm}\right]=\mp\omega\hat{\xi}_1^{\pm} . \tag{3.8}$$

Substitution of (3.1) into this equation yields, on equat-

ing powers of $\sqrt{\sigma}$, a set of equations for the WKB functions, $W_0, W_1, \ldots$. To simplify notation we set

$$\theta=\tan^{-1}x, \quad \mu=(1+x^2)^{1/2} \tag{3.9}$$

and define

$$z_\pm=\frac{iW_0^{\pm\prime}}{(1+x^2)^{1/2}} . \tag{3.10}$$

Then $z_\pm$ satisfies

$$z_\pm^3+e^{\mp i\theta}z_\pm\pm\omega=0 , \tag{3.11}$$

while the first correction $W_1^\pm$ is given by

$$\frac{iW_1^{\pm\prime}}{(1+x^2)^{1/2}}=-\frac{3z_\pm(z_\pm/\mu)'+(e^{\mp i\theta}/\mu)'}{3z_\pm^2+e^{\mp i\theta}} . \tag{3.12}$$

Note that (3.11) confirms our early anticipation that ω should scale as $1/\sqrt{\sigma}$.

Since (3.11) is a cubic, there exist three possible solutions for $W_0^{\pm\prime}$. The relevant solutions (if any) must satisfy (3.7), which implies that

$$\pm\mathrm{Im}\,z_\pm>0 . \tag{3.13}$$

Physically, we will be interested in disturbances that propagate *down* the sides of the dendrite away from the tip. Our ensuing analysis is clearer if we discuss explicitly only propagation towards $x=+\infty$. In this case, we also demand that

$$\hat{\zeta}_1(x,\omega)\to 0 \quad \text{as } x\to+\infty . \tag{3.14}$$

Hence, we require

$$\mathrm{Im}\,W^\pm>0 \quad \text{as } x\to+\infty \tag{3.15}$$

or

$$\mathrm{Re}\,z_\pm\to R_\infty<0 \quad \text{as } x\to+\infty . \tag{3.16}$$

It is possible to find the three roots of (3.11) explicitly. Define

$$\Phi^\pm=\left[\left[\frac{e^{\mp 3i\theta}}{27}+\frac{\omega^2}{4}\right]^{1/2}\mp\frac{\omega}{2}\right]^{1/3} \tag{3.17}$$

and

$$\Psi^\pm=\left[\left[\frac{e^{\mp 3i\theta}}{27}+\frac{\omega^2}{4}\right]^{1/2}\pm\frac{\omega}{2}\right]^{1/3} \tag{3.18}$$

then the three roots of (3.11) can be written

$$z_\pm^{(0)}=\Phi^\pm-\Psi^\pm , \tag{3.19a}$$

$$z_\pm^{(1)}=e^{2\pi i/3}\Phi^\pm+e^{\pi i/3}\Psi^\pm , \tag{3.19b}$$

$$z_\pm^{(2)}=e^{-2\pi i/3}\Phi^\pm+e^{-\pi i/3}\Psi^\pm . \tag{3.19c}$$

We shall make use of these exact expressions later in our numerical calculations. However, to explore the essential physical (and mathematical) content, it suffices to retain only the leading two terms in a small ω expansion. Expanding (3.19), or, more directly, (3.11) we obtain

$$z_\pm^{(0)}=\mp\omega[e^{\pm i\theta}-\omega^2e^{\pm 4i\theta}+O(\omega^4)] , \tag{3.20a}$$

$$z_\pm^{(1)}=+ie^{\mp i\theta/2}\pm\tfrac{1}{2}\omega e^{\pm i\theta}+O(\omega^2) , \tag{3.20b}$$

and

$$z_\pm^{(2)}=-ie^{\mp i\theta/2}\pm\tfrac{1}{2}\omega e^{\pm i\theta}+O(\omega^2) . \tag{3.20c}$$

Applying conditions (3.13) and (3.15), we conclude that for $\omega\ll 1$, the only acceptable solutions for $x>0$ are $z_-^{(0)}$ if $\omega>0$ and $z_+^{(0)}$ if $\omega<0$.

Integrating (3.20a) gives

$$\mathrm{Re}\,W_0^\pm=-\omega\left[\frac{x^2}{2}-\omega^2A(x)+O(\omega^4)\right] \tag{3.21}$$

and

$$\mathrm{Im}\,W_0^\pm=\pm\omega[x-\omega^2B(x)+O(\omega^4)] , \tag{3.22}$$

where

$$A(x)=12-4(1+x^2)^{1/2}-\frac{8}{(1+x^2)^{1/2}} \tag{3.23}$$

and

$$B(x)=-15s(x)+8x(1+x^2)^{1/2}+\frac{8x}{(1+x^2)^{1/2}} \tag{3.24}$$

with

$$s(x)=\tfrac{1}{2}\ln[x+(1+x^2)^{1/2}]+\tfrac{1}{2}x(1+x^2)^{1/2} . \tag{3.25}$$

For future convenience, we have adjusted the constant of integration so that $W_0^\pm(x=0,\omega)=0$. It is straightforward to check that $\mathrm{Im}W_0^-$ ($\mathrm{Im}W_0^+$) has the correct behavior along the deformed contour for $\omega>0$ ($\omega<0$) to justify our estimation of the integrals in (2.11) and (2.12). As $x\to+\infty$,

$$A(x)=-4x+O(1) \tag{3.26}$$

and

$$B(x)=\tfrac{1}{2}x^2+O(\ln x) . \tag{3.27}$$

The leading terms in (3.21) and (3.22) imply that

$$\hat{\zeta}_1^-(x,\omega)\sim e^{i\omega(t-x^2/2)/\sqrt{\sigma}}e^{\omega[x-\omega^2B(x)]/\sqrt{\sigma}} , \tag{3.28}$$

which, as required, describes a perturbation that propagates towards $x=+\infty$. However, while $\hat{\zeta}_1^-$ ultimately decays in accord with (3.14), initially the perturbation is *amplified*. Moreover, for small ω this amplification increases with ω. We also observe that the speed of propagation down the dendrite is unity so that the perturbation remains stationary in the laboratory frame.

We can similarly expand (3.19) for large ω. The three solutions are then

$$z_\pm^{(k)}=\mp\omega^{1/3}e^{\mp 2\pi ik/3}\pm\tfrac{1}{3}\omega^{-1/3}e^{\pm 2\pi ik/3}e^{\mp i\theta}+O(\omega^{-5/3}) . \tag{3.29}$$

Again, applying (3.13) and (3.16), we find that only one of these solutions is acceptable. For $x>0$ and $\omega\gg 1$ this is $z_-^{(2)}$, which gives

$$iW_0=-\tfrac{1}{2}s(x)\omega^{1/3}(1+i\sqrt{3})+O(\omega^{-1/3}) , \tag{3.30}$$

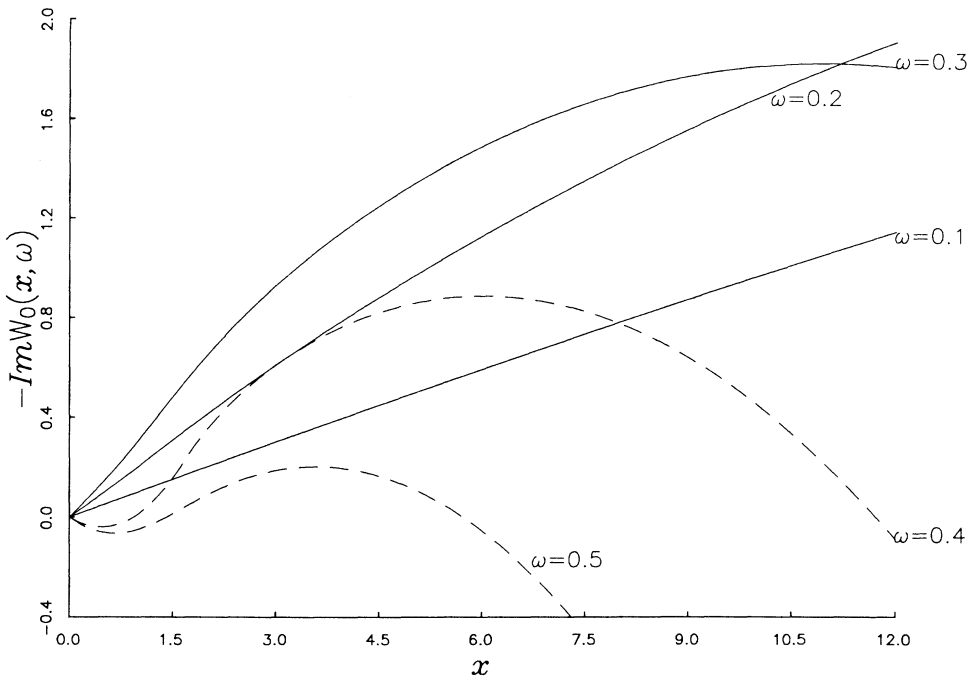

FIG. 1. Plot of $-\mathrm{Im}W_0(x)$ as a function of x for the indicated values of ω.

where $s(x)$, defined in (3.25), is the arc length down the dendrite. (For $\omega \ll -1$, the appropriate solution is $z_+^{(2)}$.) Since the real part of (3.30) is negative for all x, there is, in this case, no amplification of the perturbation as occurs for small ω.

The preceding analysis establishes the existence of a single acceptable WKB solution to (3.8) for sufficiently small and sufficiently large ω. However, the solutions in these two limits correspond to *different* roots of (3.11). Inspection of (3.17) or (3.18) shows that the determinant of this selection is the phase of the square root appearing in $\Phi^{\pm}$ and $\Psi^{\pm}$. Hence, we expect that $z_-^{(0)}$ remains the relevant solution for all $\omega < \omega_c$, where

$$\omega_c^2 = 4/27 \ . \tag{3.31}$$

At this critical value, the two WKB solutions become degenerate at $\theta = \pi/3$ (or $x = \sqrt{3}$). As ω passes through ω_c, $z_-^{(0)}$ and $z_-^{(2)}$ exchange their validity with respect to condition (3.16).

For $\omega < \omega_c$, $z_-^{(0)}$ is such that the resulting solution $\hat{\xi}_1(x,\omega)$ converges at infinity, whereas the solution derived from $z_-^{(2)}$ diverges. For $\omega > \omega_c$, $z_-^{(2)}$ yields the convergent solution for $\hat{\xi}_1$. This switch of the physically relevant solutions has a marked effect on the response of the dendrite to a perturbation of given frequency. This can be seen in Fig. 1, where we plot $-\mathrm{Im}W_0(x)$ as function of x for different values of ω with W_0 constructed by integrating the appropriate root, $z_-^{(0)}$ or $z_-^{(2)}$, of (3.11). This figure is essentially, apart from a scaling by $1/\sqrt{\sigma}$, a plot of the logarithm of the amplitude of $\hat{\xi}_1(x,\omega)$. The amplification implied by (3.22) for small ω is apparent. The qualitative change in the response as ω passes through ω_c is also apparent. Strikingly, we observe that for ω slightly greater than ω_c the perturbation is first suppressed then magnified before ultimately decaying.

It should be stressed, however, that the naive WKB analysis that we have carried out breaks down in a neighborhood in the complex x plane of $x = \sqrt{3}$ for $\omega \sim \omega_c$. We discuss this point further in Sec. IV. In particular, one would expect that the derivative of exact solution of (3.8) near $x = 0$ to vary smoothly with ω rather than discontinuously as suggested by Fig. 1.

With W_0 evaluated, we can, in principle, compute W_1 from (3.12). For small ω, we obtain by substituting (3.20a) in (3.12) and integrating

$$iW_1^{\pm} = \ln(1 \pm ix) - 2\omega^2(e^{\pm 3i\theta} - 1) + O(\omega^4) \ , \tag{3.32}$$

where we have again set the constant of integration so that $W_1^{\pm}(x=0,\omega)=0$.

IV. COMPARISON WITH NUMERICAL RESULTS

In this section we compare our analytical results with the numerical analysis presented in a recent paper by Kessler and Levine.[14] As we shall see, we can reproduce with a satisfactory quantitative agreement all the qualitative features emphasized by Kessler and Levine, although we must admit that, in view of our analytical results, the sidebranching wavelength selection mechanism proposed by those authors does not seem to be completely well defined. In order to make the comparison more transparent, we switch, in this section, to the notation used by Kessler and Levine, whose length and time units are $l = 2D/v$ and l/v, respectively; l being the diffusion length.

The numerical study refers to the normal displacement $\delta(u)$ of the steady-state interface when the system is forced at a particular frequency Ω. [The parameter u is defined below in (4.2).] This is the same as solving (2.8), with the difference that while we treat both the steady-state shape correction and the time-dependent perturbation to linear order, only the latter is considered small in the numerical analysis of Ref. (14) where linearization is performed about the full steady-state solution. For those values of parameters that we are interested in, this should not make an appreciable difference.[20] To first order in $\hat{\xi}_1(x,\omega)$ one can easily check that

$$\delta(u)=\frac{\hat{\xi}_1(x(u),\omega)}{[1+x^2(u)]^{1/2}} , \tag{4.1}$$

where the relation between x and u as defined by Kessler and Levine is

$$u=\tfrac{1}{2}p[(1+2x^2)^2-1]^{1/2} . \tag{4.2}$$

Note that p accounts for the change in length unit and that u is a simple interpolation of the relation [see (3.25)] between x and the arc length s along the Ivantsov parabola. If $x \ll 1$ then $u \simeq s$, while for $x \gg 1$ we have $u \simeq 2s$. Finally the relation between ω and Ω is easily computed to be $\omega = p\sqrt{\sigma}\Omega$.

All the qualitative features of the numerical study of the sidebranching modes are actually evident already in Fig. 1 of the preceding Sec. III, which is a plot of $\mathrm{Re}[iW_0^-(x,\omega)]$. More quantitatively, for small ω we have, to order ω^3, from (3.24) and (3.28):

$$\mathrm{Re}\left[\frac{iW_0^-(x,\omega)}{\sqrt{\sigma}}\right] \sim \frac{\omega}{\sqrt{\sigma}}\left[x-\omega^2\left[\frac{x}{2}(1+x^2)^{1/2}+\frac{8x}{(1+x^2)^{1/2}} -\tfrac{15}{2}\ln[x+(1+x^2)^{1/2}]\right]\right] . \tag{4.3}$$

We explicitly see that the sidebranching mode $\hat{\xi}_1(x) \sim \exp(iW_0^-/\sqrt{\sigma})$ is exponentially amplified in a region that, for $\omega \ll 1$, extends to $x \simeq 1/\omega^2$. For x greater than this, the amplitude decreases and eventually dies away. This is illustrated in Fig. 2, which is a plot of $\mathrm{Re}\delta(u)$ as a function of the arc length parameter, u, for $\Omega=25$ and $\sqrt{\sigma}=0.13$.

On the other hand, if we fix x and consider the response as a function of ω, we find that the amplification has a peak at $\omega_p^2 \simeq 2/3x$. Because of this x dependence, it is not obvious to us how one should select the value of ω responsible for the experimentally observed sidebranching wavelength. Indeed, for $0<\omega<\omega_c$ all modes are characterized by exponential amplification and we can check explicitly that the quasistationary ap-

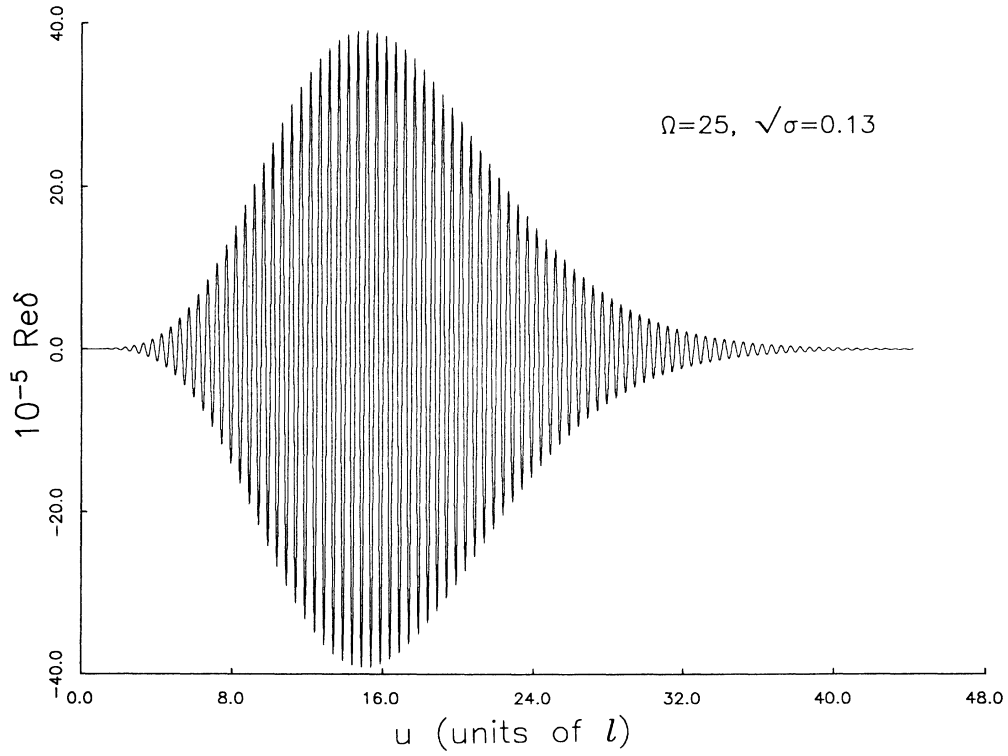

FIG. 2. Response of the dendrite to a fixed frequency ($\Omega=25$). The curve is a plot of $\mathrm{Re}\delta(u)=\mathrm{Re}[\exp(iW_0/\sqrt{\sigma}+iW_1)]$ as a function of the arc length parameter u for $\sqrt{\sigma}=0.13$ and $p=0.08$. The functions $W_0(x)$ and $W_1(x)$ were obtained by extending their small ω expansions (see Sec. III) to fourth order. (Note that the abscissae are in units of the diffusion length.)

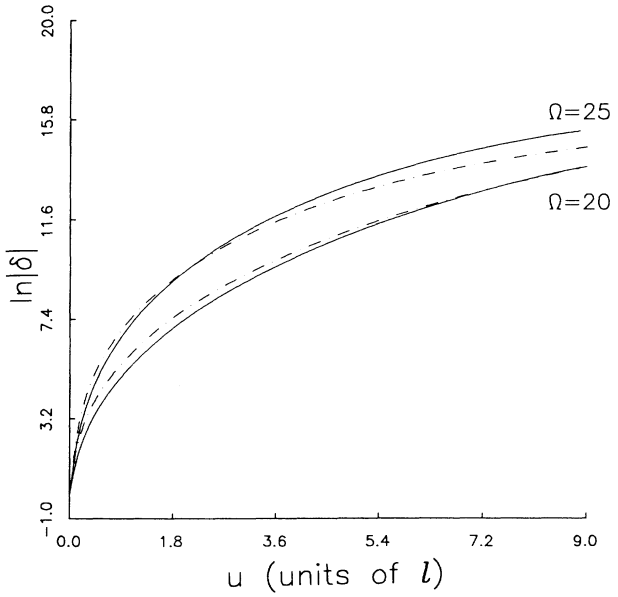

FIG. 3. Amplification, $\ln|\delta(u)|$, of fixed frequency perturbations as a function of distance, measured by parameter u, see (4.2), from the tip. The solid curves are the WKB approximations for $\delta(u)$ obtained by numerically integrating (3.20a) and (3.12) for W_0 and W_1. The dashed curves are the corresponding numerical calculations of Kessler and Levine (Ref. 14). The system parameters pertaining to the plot are $\sigma=0.017$ and $p=0.08$.

proximation is satisfied by these modes if $\omega > p\sqrt{\sigma}$. As we will see in Sec. V, this whole band of values of ω is relevant to the propagation of localized wave packets.

In Fig. 3 we directly compare our result for the logarithm of the amplitude $\log|\delta(u)|$ with the numerical data of Kessler and Levine. The values of Ω chosen are 20 and 25 and correspond[21] to values of ω given approximately to 0.21 and 0.26. The quantitative agreement, which is quite satisfactory for these and smaller values of ω, is not so good when ω gets closer to ω_c. The reason for this disagreement is easy to understand. As mentioned in Sec. III, the WKB analysis breaks down in a neighborhood of the point $x=\sqrt{3}$ in the complex x plane when $\omega \simeq \omega_c$. Indeed the relevant turning point of (3.8) moves from $x=i$ through $x=\sqrt{3}$, at $\omega=\omega_c$, to $x=-i$ when ω goes from 0 to $+\infty$. Our analysis, however, completely neglects this fact; essentially because we are mainly interested in values of ω such that $\omega \ll \omega_c$ and, in this regime, our solution is uniformly valid for all positive x.

A more careful examination of (3.8) when ω is in a neighborhood of ω_c would also presumably smooth away the discontinuous behavior of the solution close to ω_c that has been discussed in Sec. III and can be seen in Fig. 1. Such a detailed analysis, however, although mathematically interesting is somewhat unnecessary from our point of view as will appear more clearly from the analysis of Sec. V.

V. EVOLUTION OF A WAVE PACKET

Our analysis in Sec. III and the discussion of Sec. IV has concerned the evolution of a perturbation of *fixed* frequency. It is more relevant physically to consider small perturbations of the steady-state needle crystal that are localized in space and propagate down the dendrite. Hence, we define a *wave packet*

$$\zeta_1(x,t)=\int_{-\infty}^{\infty} d\omega\, F(\omega)\hat{\zeta}_1(x,\omega)e^{i\omega t/\sqrt{\sigma}}\ , \tag{5.1}$$

where we assume that $F(\omega)=F(-\omega)$ is smooth and broad and that $\hat{\zeta}_1$ has the WKB form (3.1). Again, in the spirit of Sec. III, we shall restrict attention to the propagation of this pulse towards $x=+\infty$.

We focus on the behavior of the wave packet after it has moved well away from its initial position near the tip. Our results of Sec. III imply that for $x,t \gg 1$, the wave packet will find itself in regime such that only small values of ω contribute to the integral in (5.1). We can thus simplify the discussion by making use of the small ω expressions, (3.21), (3.22), and (3.32), for the WKB functions, where W^- is the relevant solution for $\omega>0$ and W^+ that for $\omega<0$. Since $iW^+(x,-\omega)=[iW^-(x,\omega)]^*$, where $*$ denotes complex conjugation, we can write (5.1) as

$$\zeta_1(x,t)=2(1+x^2)^{1/2}\mathrm{Re}\left[e^{-i\theta}\int_0^{\infty} d\omega\, F(\omega)e^{\omega[x-\omega^2 B(x)]/\sqrt{\sigma}}e^{i\omega[t-\bar{z}+\omega^2 A(x)]/\sqrt{\sigma}}\right]\ , \tag{5.2}$$

where the functions $A(x)$ and $B(x)$ are given by (3.23) and (3.24), respectively. In writing (5.2), we have also neglected the term of order ω^2 in W_1; an omission that will be justified by the following analysis. We have also defined

$$\bar{z}=\tfrac{1}{2}x^2\ , \tag{5.3}$$

which for large x is simply the arc length s, recall (3.25), along the dendrite from the tip to the point $(x,\bar{z})$. We shall find that the most important regime is $\bar{z}\sim t$.

We now estimate the integral over ω in (5.2) by a saddle point approximation. The saddle point frequency is

$$\omega_s=\frac{1}{\sqrt{3}}\left[\frac{2}{\bar{z}}\right]^{1/4}\left[1-i\frac{\bar{z}-t}{\sqrt{2\bar{z}}}\right]^{1/2}+O(\bar{z}^{-5/4})\ , \tag{5.4}$$

where the second term can be neglected for $(\bar{z}-t)^2 \ll \bar{z}$, thereby substantiating our use of the small ω expansions in (5.1) and the neglect of all ω dependence in W_1. Hence we obtain

$$\zeta_1(x,t)\sim f(2\bar{z})^{1/8}\sigma^{1/4}\mathrm{Im}\exp\left[\frac{(2\bar{z})^{1/4}}{c^3\sqrt{\sigma}}\left[1-i\frac{\bar{z}-t}{\sqrt{2\bar{z}}}\right]^{3/2}\right], \tag{5.5}$$

where $c=\sqrt{3/2}$ and f is a numerical constant of order unity. For $(\bar{z}-t)^2\ll\bar{z}$ this simplifies to

$$\zeta_1(x,t)\sim f(2\bar{z})^{1/8}\sigma^{1/4}\sin\left[\frac{(t-\bar{z})}{c\sqrt{\sigma}(2\bar{z})^{1/4}}\right]\exp\left[\frac{(2\bar{z})^{1/4}}{c^3\sqrt{\sigma}}-\frac{(\bar{z}-t)^2}{4c\sqrt{\sigma}(2\bar{z})^{3/4}}\right]. \tag{5.6}$$

This result describes an exponentially growing wave packet, whose amplitude varies as $\exp(a\bar{z}^{1/4}/\sqrt{\sigma})$, where a is a positive constant. From the exponential factor in (5.6), we observe that the pulse is centered at $x\simeq t$ so that it moves down the dendrite at unit velocity, that is, it remains stationary in the laboratory frame. However, the width of the packet increases as

$$\Delta x\sim 2c^{1/2}\sigma^{1/4}(2\bar{z})^{3/8}, \tag{5.7}$$

and the wavelength

$$\lambda\sim 2\pi c\sqrt{\sigma}(2\bar{z})^{1/4} \tag{5.8}$$

is also weakly x dependent.

Two features of the wave packet described by (5.6) are worth specific comment at this time. Firstly, the dependence of the amplitude, width, and wavelength on σ and on $\bar{z}$ is *identical to that found*[15] *in the boundary-layer model.*[4] Secondly, in contrast to the fixed frequency response discussed in Secs. III and IV, the disturbance continues to grow at arbitrarily large distances down the dendrite. This growth is a consequence of our assumption that the initial pulse contained arbitrarily small frequencies. It is only these components of lower and lower frequency that continue to grow unstably by the process described in Sec. III as $\bar{z}$ increases.

VI. SUMMARY AND DISCUSSION

In this paper we have discussed the evolution of time-dependent perturbations of the needle crystal solution of the two-dimensional symmetric model of solidification. Within a WKB approximation we found that a *selective amplification mechanism* results in the initial amplification of a perturbation of fixed frequency ω (less than some critical frequency ω_c) as it propagates down the dendrite. However, ultimately such a perturbation dies out. On the other hand, a wave packet that is initially localized close to the tip will continue to grow exponentially as the pulse moves to arbitrarily large distances from the tip provided the initial wave packet contains modes of arbitrarily small frequency. Our analysis predicts that the amplitude of the packet grows as $e^{as^{1/4}\sigma^{-1/2}}$, where a is a positive constant, σ is a dimensionless surface tension parameter, and s is the arc length down the dendrite. The characteristic wavelength associated with the packet varies as $\sigma^{1/2}s^{1/4}$, while its width varies as $\sigma^{1/4}s^{3/8}$; recall (5.7) and (5.8). Typically, $\sigma\sim 0.02$.

At this point a comment is appropriate on the closely related work of Pelcé[22] and Caroli *et al.*[17] using the Zel'dovich[23,24] method. Pelcé's initial perturbation does not contain low-frequency components. Consequently, he concludes that the perturbation dies out at large $\bar{z}$. On the other hand, Caroli *et al.*[17] discuss the evolution of a localized front deformation. The starting point of this analysis is a linearized equation that appears to account, rather generally, for the effects of the initial shape correction and temperature field perturbations. However, some of the subsequent approximations introduced to make this equation mathematically tractable are completely equivalent to simply replacing it with our equation (2.8). Caroli *et al.* then essentially assume a solution of the form $\zeta_1(x,t)=e^{S(x,t)}$, where

$$S(x,t)=f(t)+iq(t)[x-x_0(t)]-\tfrac{1}{2}\alpha(t)[x-x_0(t)]^2, \tag{6.1}$$

and derive equations for the functions $f(t)$, $q(t)$, $x_0(t)$, and $\alpha(t)$. While this ansatz is precisely of the same form as our *final* result (5.6) for the wave packet and the predictions for the behavior of the width and the characteristic wavelength agree, apart from a numerical factor, with our results (5.7) and (5.8), the two analyses are, in fact, rather different. One reflection of this difference occurs in the amplification of the wave packet; Caroli *et al.* do not obtain the exponential amplification that we predict. The origin of the differences in the two techniques seems to be fundamental. The analytical techniques of Caroli *et al.* do not appear capable of treating correctly the small ω modes, essential for the amplification. The power of the WKB method we have used, in contrast to a Zel'dovich approach, is that it does not force us to consider an initial perturbation which is localized on the scale of the tip radius. This is quite important since, from the discussion in Sec. V. it is the very long wavelength components of the initial perturbation that are crucial in determining the amplification of the packet, rather than the "most dangerous" initial modes as assumed by Caroli *et al.*

As remarked in Sec. V, our results on the propagation of a wave packet are identical, as far as their dependence on σ and s are concerned, as those found[15] in the boundary-layer model.[4] Despite the neglect of nonlocal effects in its treatment of the thermal field, this model appears to retain faithfully many of the essential effects and features of more realistic models.

Our results for the propagation of fixed frequency modes for sufficiently small frequency *quantitatively* reproduce all of the features found in a recent numerical study[14] of the same problem. At higher frequencies, the

agreement is only qualitative due to a breakdown of our WKB analysis. It is conceivable that this could be rectified by a more detailed analysis of the WKB solutions. We have not carried this out since we believe that the evolution of wave packets is more relevant to sidebranching in dendrites than the evolution of fixed frequency perturbations.

The picture we have of the generation of sidebranches is as follows. The growing needle crystal is perturbed locally by some external noise, presumably simple broadband thermal noise. Perturbations arising near the tip propagate down the sides of the dendrite and undergo amplification as described above resulting in the ultimate development of visible sidebranches some distance from the tip. It is precisely this scenario that was suggested by the boundary-layer model results.[15] In view of the quantitative agreement between our results for the symmetric model and corresponding calculations in the boundary-layer model, it is very plausible that a noise-driven sidebranching mechanism is also valid. To confirm this expectation requires the explicit inclusion of noise into our calculations. Since the symmetric model is based on a completely realistic description of the thermal field there is in principle no difficulty in adding such thermal fluctuations. However, there are very definite technical difficulties. Some progress is possible and this is described in a separate report.[19]

One of the most satisfying aspects of the calculations reported in this paper is the extent to which it is possible to carry out an *analytical* treatment of what is a rather difficult nonlocal problem [recall (2.1)]. Our results, together with earlier results on steady-state velocity selection[10] in dendrites and related work[24,25] on viscous fingering in the Saffman-Taylor[26] problem, confirm that such WKB approximations are very powerful methods for the discussion of such singularly perturbed nonlinear problems.

We conclude by commenting specifically on one recent other application[16] of this approach that is very similar to the calculations reported in this paper. Bensimon *et al.*[16] discuss the stability against short wavelength perturbations of moving curved fronts in both the dendrite problem and the Saffman-Taylor problem. While their basic equation is very similar to, but slightly simpler than, our equation (2.8), their resulting equation for the dominant WKB solution, W_0 in our notation, is identical to our equation (3.11) with again two possible solutions, the analogs of $z_{-}^{(0)}$ and $z_{-}^{(2)}$ of Sec. III. The difference is that Bensimon *et al.* consider pure imaginary $\omega\ (=iv)$ corresponding to the so-called tip-splitting modes. As a result, the boundary conditions they impose are different, namely, modes must vanish as x tends to both $+\infty$ and $-\infty$. They find that acceptable solutions exist now only for select values of v. These values are determined by a resonance condition similar to the Bohr-Sommerfeld quantization relation, the derivation of which involves a subtle consideration of the behavior of the WKB functions in the complex plane. This analysis is similar to that one would need to perform to accurately describe the behavior of sidebranching modes with frequencies $\omega \sim \omega_c = 2/3\sqrt{3}$. While of interest mathematically, such an analysis is of less relevance physically given the conclusions reached in Sec. V concerning the motion of spatially localized wave packets.

ACKNOWLEDGMENTS

The authors thank Dr. H. Levine for making available data from his numerical calculations to facilitate the comparison described in Sec. IV. This research was supported by the U.S. Department of Energy under Grant No. DE-FG03-84ER45108 and by the National Science Foundation under Grant No. PHY-82-17853, supplemented by funds from the U.S. National Aeronautics and Space Administration, at the University of California at Santa Barbara.

*Permanent address: Department of Mathematics, The Faculties, The Australian National University, Canberra, Australian Capital Territory 2600, Australia.

[1]J. S. Langer, Lectures in the Theory of Pattern Formation, Les Houches Summer School, Chance and Matter, July 1986 (unpublished).

[2]G. P. Ivantsov, Dokl. Akad. Nauk SSSR **58**, 567 (1947).

[3]R. Brower, D. Kessler, J. Koplik, and H. Levine, Phys. Rev. Lett. **51**, 111 (1983); Phys. Rev. A **29**, 1335 (1984); D. Kessler, J. Koplik, and H. Levine, *ibid.* **30**, 3161 (1984); **31**, 1712 (1985).

[4]E. Ben-Jacob, N. Goldenfeld, J. S. Langer, and G. Schon, Phys. Rev. Lett. **51**, 1930 (1983); Phys. Rev. A **29**, 330 (1984); E. Ben-Jacob, N. Goldenfeld, B. G. Kotliar, and J. S. Langer, Phys. Rev. Lett. **53**, 2110 (1984).

[5]J. S. Langer, Phys. Rev. A **33**, 435 (1986).

[6]J. S. Langer and D. C. Hong, Phys. Rev. A **33**, 435 (1986).

[7]D. Meiron, Phys. Rev. A **33**, 2704 (1986).

[8]D. Kessler and H. Levine, Phys. Rev. A **33**, 7867 (1986).

[9]B. Caroli, C. Caroli, B. Roulet, and J. S. Langer, Phys. Rev. A **33**, 442 (1986).

[10]A. Barbieri, D. Hong, and J. S. Langer, Phys. Rev. A **35**, 1802 (1987).

[11]P. Pelcé and Y. Pomeau, Stud. Appl. Math. **74**, 245 (1986).

[12]B. Caroli, C. Caroli, C. Misbah, and B. Roulet (unpublished).

[13]See, e.g., J. S. Langer, Rev. Mod. Phys. **52**, 1 (1980).

[14]D. Kessler and H. Levine, Europhys. Lett. (to be published).

[15]R. Pieters and J. S. Langer, Phys. Rev. Lett. **56**, 1948 (1986).

[16]D. Bensimon, P. Pelcé, and B. I. Shraiman (unpublished).

[17]B. Caroli, C. Caroli, and B. Roulet (unpublished).

[18]W. W. Mullins and R. F. Sekerka, J. Appl. Phys. **35**, 444 (1964).

[19]J. S. Langer, following paper, Phys. Rev. A **36**, 3350 (1987).

[20]J. S. Langer and H. Müller-Krumbhaar, Acta Metall. **26**, 1697 (1978).

[21]The relevant system parameters are, in our notation, $\sigma \simeq 0.017$ and $p = 0.08$. The numerical data also pertain to a small fourfold crystal anisotropy, $\epsilon = 0.1$. As discussed above we do not expect this to cause a significant discrepancy.

[22]P. Pelcé, thèse, Université de Provence (1986).

[23]Ya. B. Zel'dovich, A. G. Istratov, N. I. Kidin, and V. B. Li-

brovich, Combust. Sci. Technol. **24**, 1 (1980).
[24]D. Bensimon, L. P. Kadanoff, S. Liang, B. I. Shraiman, and C. Tang, Rev. Mod. Phys. **58**, 977 (1986).
[25]B. I. Shraiman, Phys. Rev. Lett. **56**, 2028 (1986); R. Combescot, T. Dombre, V. Hakin, Y. Pomeau, and A. Pumir, *ibid.* **56**, 2036 (1986); D. C. Hong and J. S. Langer, *ibid.* **56**, 2082; and Phys. Rev. A **36**, 2325 (1987).
[26]P. G. Saffman and G. I. Taylor, Proc. R. Soc. London, Ser. A **245**, 312 (1958).